

Materials and Methods

Animal experiments

The intestinal specific SIRT1 knockout mice (SIRT1 iKO) in a C57BL/6 background were generated by crossing mice carrying a SIRT1 exon 4 floxed allele (Cheng et al, 2003) with mice expressing Cre recombinase driven by the Villin promoter (Jackson laboratory). Three to four-month old SIRT1 iKO mice (Villin-Cre⁺, SIRT1^{flox/flox}) and their age-matched littermate Flox controls (Villin-Cre⁻, SIRT1^{flox/flox}), as well as wild type (Villin-Cre⁻, SIRT1^{+/+}) and Villin-Cre (Villin-Cre⁺, SIRT1^{+/+}) control mice, were fed ad libitum either a standard laboratory chow diet, a chow diet containing 0.5% cholic acid (Research Diets, custom made), a chow diet containing 1.25% Cholesterol (Research Diets, custom made), or a lithogenic diet (D12383, Research Diets) for indicated times. All animal experiments were approved by the NIEHS/NIH Animal Care and Use Committee.

Histological and biochemical analysis

Paraffin-embedded intestine and liver sections were stained with hematoxylin and eosin (H&E) for morphology. The liver sections were examined by a board certified veterinary pathologist and were graded using the criteria proposed by Kleiner et al. (1) for scoring the hepatic lesions in non-alcoholic fatty liver disease (NAFLD).

Serum LDL, HDL and total cholesterol and triglycerides were measured using commercially available kits (Wako and Sigma). Serum Alanine transaminase (ALT) and aspartate aminotransferase (AST) activities were measured using the ALT and AST kits from Catechem.

To analyze crypt-cell proliferation and apoptosis, paraffin-embedded mouse intestine tissues sections were stained for BrdU to study proliferation and with caspase-3 to study cell death. For BrdU staining, mice were sacrificed 90 min after i.p. injection of 5-bromo-2'-deoxyuridine (BrdU) (Amersham), BrdU incorporation in crypt cells was measured in intestinal sections. For caspase-3 staining, intestinal sections were incubated with rabbit anti-ACTIVE® Caspase-3 antibody (G7481, Promega, Madison, WI), then incubated with Rabbit on Rodent HRP-Polymer (Biocare). The signal was visualized with 3,3-diaminobenzidine (Dako, Carpinteria, CA).

To determine the fecal bile acid outputs, feces were collected from individually housed mice over 48 h and bile acids from feces were extracted with 75% ethanol at 50 °C for 2 h, followed by centrifugation at 1500 g for 10 min. Bile acids were then measured in the resulting supernatants with the total bile acid kit based on 3 α -hydroxysteroid dehydrogenase (Diazyme Laboratories).

To determine the fecal cholesterol outputs, total cholesterol were extracted from feces and analyzed by the Agilent 6890N GC systems at the Wake Forest School of Medicine Lipoprotein Analysis Laboratory.

To determine the total bile acid pool size, liver, gall bladder, and full-length small intestine were dissected and homogenized in water, and bile acids were then extracted with 75% ethanol as described above.

Everted gut sac experiment

The everted gut sac experiments were carried out essentially as described in (2). Briefly, the small intestines dissected from Flox and SIRT1 iKO mice were divided into four equal segments and rinsed with cold PBS, and a 7-cm segment from each segment was weighed, gently everted, filled with Krebs Ringer Buffer (KRB), and closed using suture. The closed sacs were incubated for 30 min at 37°C in oxygenated KRB plus 25 μ M [3 H] taurocholate (Perkin–Elmer) and 180,000 dpm/ml of inulin [14 C] carboxylic acid (Amersham Biosciences, as a marker for integrity of the gut sac and for paracellular movement). After incubation, the sacs were removed, rinsed in ice-cold KRB, and weighed, and the serosal fluid was recovered. The empty sac was solubilized, and aliquots of mucosal fluid, serosal fluid, and sac tissue extract were taken to measure radioactivity.

RNA analysis

Total RNA was isolated from cells or tissues using Trizol (Invitrogen) and Qiagen RNeasy mini-kit (Qiagen). For quantitative real-time PCR (qPCR), cDNA was synthesized with the ABI reverse transcriptase kit, and analyzed using SYBR Green Supermix (Applied Biosystems). All data were normalized to

Lamin A expression.

Chromatin immunoprecipitation (ChIP) analysis

Chromatin immunoprecipitation (ChIP) analysis was performed essentially as described by the manufacturer, EMD Millipore (Upstate Biotechnology). Briefly, Flox and SIRT1 iKO mice were perfused with 1% paraformaldehyde in PBS at room temperature via heart perfusion to cross-link protein-DNA complexes. After 10 min, the cross-linking was stopped by perfusion with 0.125 M glycine. The cross-linked ileum was minced and dounced in SDS lysis buffer (50 mM Tris-HCl, pH 8.1, 10 mM EDTA, 1% SDS, and 2xComplete™ protease inhibitor mixture). Chromatin was then sonicated to an average length of 200-500 bp and subjected to immunoprecipitation with antibodies against FXR, HNF1 α (Santa Cruz biotechnology), or normal rabbit IgG. DNA fragments were subjected to qPCR using primers flanking indicated promoter regions.

Luciferase assay

For trans-activation experiments, the mouse FXR promoter (-2644 to +149 fragment) was cloned into the pGL3 basic vector (Promega). The mouse Asbt promoter luciferase reporter construct has been described before (3). For luciferase assay in Hepa1-6 cells, Hepa1-6 were electroporated with negative control siRNA or siRNA against HNF1 α . Two days later, cells were then transfected with the mouse FXR promoter luciferase reporter and control pRL-CMV reporter (Renilla Luciferase, Promega) together with indicated constructs,

and were cultured for 24 h before harvesting for luciferase assay. For luciferase assay in IEC-6 cells, IEC-6 cells were infected with lentiviruses expressing GFP, or WT or KQ DCoH2 proteins for 24 hours. Cells were then transfected with luciferase reporters for mouse FXR or Asbt promoters and control pRL-CMV reporter together with or without HA-HNF1 α expressing construct and harvested 2 days later for luciferase assay. Luciferase activity was measured using the Dual-Luciferase Reporter Assay System (Promega). The final firefly luciferase activity was normalized to the co-expressed renilla luciferase activity.

Protein acetylation analysis

To analyze the deacetylation of DCoH2 by SIRT1, HEK293T SIRT1RNAi cells were transfected with constructs expressing HA-DCoH2, with or without FLAG-p300 and SIRT1 as indicated. 48 h after transfection, cells were treated with 5 μ M TSA for 2 hours, harvested, and homogenized. HA-DCoH2 was immuno-purified from cell extracts with anti-HA beads (Santa Cruz biotech), subjected to SDS-PAGE, and analyzed with anti-acetyl-lysine polyclonal antibodies (Cell Signaling Technology Inc.).

Identification of lysine acetylation sites in DCoH2 protein

The lysine acetylation sites in DCoH2 protein were identified by a proteomics screening. In this experiment, the protein whole-cell lysate of MEF cells was prepared and digested with trypsin. The tryptic peptides were subjected to immunoprecipitation using anti-acetyllysine antibody-conjugated agarose

beads (PTM Biolabs, Inc. (Chicago, IL)) for enriching lysine acetylated peptides (4). The resulting immunoprecipitated peptides were analyzed by nano-HPLC/LTQ Orbitrap Velos mass spectrometer. The MS/MS data were analyzed by Mascot algorithm to identify lysine acetylated peptides. The candidate peptides were verified by a manual method previously reported (5). The analysis identified two acetylated sites (at K124 and K131) in DCoH2 (Figure S4).

Supplemental Figure Legend

Figure S1 Intestine-specific deletion of SIRT1 does not alter intestinal morphology under normal feeding conditions. (A) SIRT1 protein levels in different segments of intestine. The intensity of SIRT1 and actin proteins was quantified by ImageJ (n=4-9, *p<0.05). (B) SIRT1 iKO mice have normal mRNA levels of an enterocyte marker, sucrase isomaltase (Si) in different segments of small intestine (n=4). (C) SIRT1 iKO mice have normal expression levels of other intestinal epithelial cell markers in jejunum (n=4). (D) Flox and SIRT1 iKO mice display a comparable rate to transport [¹⁴C] inulin carboxylic acid, a polysaccharide consisting of five-membered furanose rings, across the small intestinal membrane in the everted gut sac assay *in vitro*, indicating a normal barrier function of SIRT1 deficient small intestine (n=9). Relative transport amount were calculated by setting the transport rate in duodenum as 1. Please note that although inulin has been routinely used as a “nonabsorbable” marker, the intestinal epithelium does absorb significant amount of inulin as reported previously (6, 7).

Figure S2 Serum triglyceride (A), cholesterol (B), HDL (C), and LDL (D) levels in Flox and SIRT1 iKO mice (n=6-8, *p<0.05).

Figure S3 Relative mRNA levels of FXR (A), SHP (B), FGF15 (C), Asbt (D), and OST α (E) in different segments of small intestine in Flox and SIRT1 iKO mice on a chow diet (n=4, matched littermate pairs, *p<0.05, # 0.05<p<0.10).

Figure S4 Mapping of acetylation on lysine residues at K124 (**A**) and at K131 (**B**) on DCoH2 protein by tandem mass spectrometry.

Figure S5 DCoH2 is an acetylation protein that regulates HNF1 α dimerization and transactivation. (A) Crystal structures of DCoH2 homo-tetramer (left, PDB entry ID 1RU0) and DCoH1/HNF1 2:2 tetramer (right, PDB entry ID 1F93). Please note that the K124 and K131 residues in the DCoH2 protein are located on the protein surface (8). (B) Two additional experiments indicate that acetylation status of DCoH2 affects HNF1 α dimerization in HEK293T cells.

Figure S6 Loss of SIRT1 in intestine results in increased hepatic bile acid synthesis after a 6-day of high-cholesterol diet feeding. (A) Serum bile acids and cholesterol levels (n=6-8). (B) SIRT1 iKO mice have increased levels of Cyp7a1 after high-cholesterol diet feeding (n=6-8). (C) SIRT1 iKO mice have increased levels of hepatic bile acids yet decreased hepatic cholesterol after high-cholesterol diet feeding (n=6-8) *p<0.05, # 0.05<p<0.10.

Figure S7 Loss of SIRT1 in intestine results in altered systemic bile acid metabolism upon lithogenic diet feeding. (A) Body weight gain and food intake of Flox control and SIRT1 iKO mice (n=7) fed a lithogenic diet (LD). (B) Serum lipid levels in Flox control and SIRT1 iKO mice during 7-week of LD feeding (n=6-8). (C) Hepatic histological lesions in Flox and SIRT1 iKO mice after 7 weeks of LD

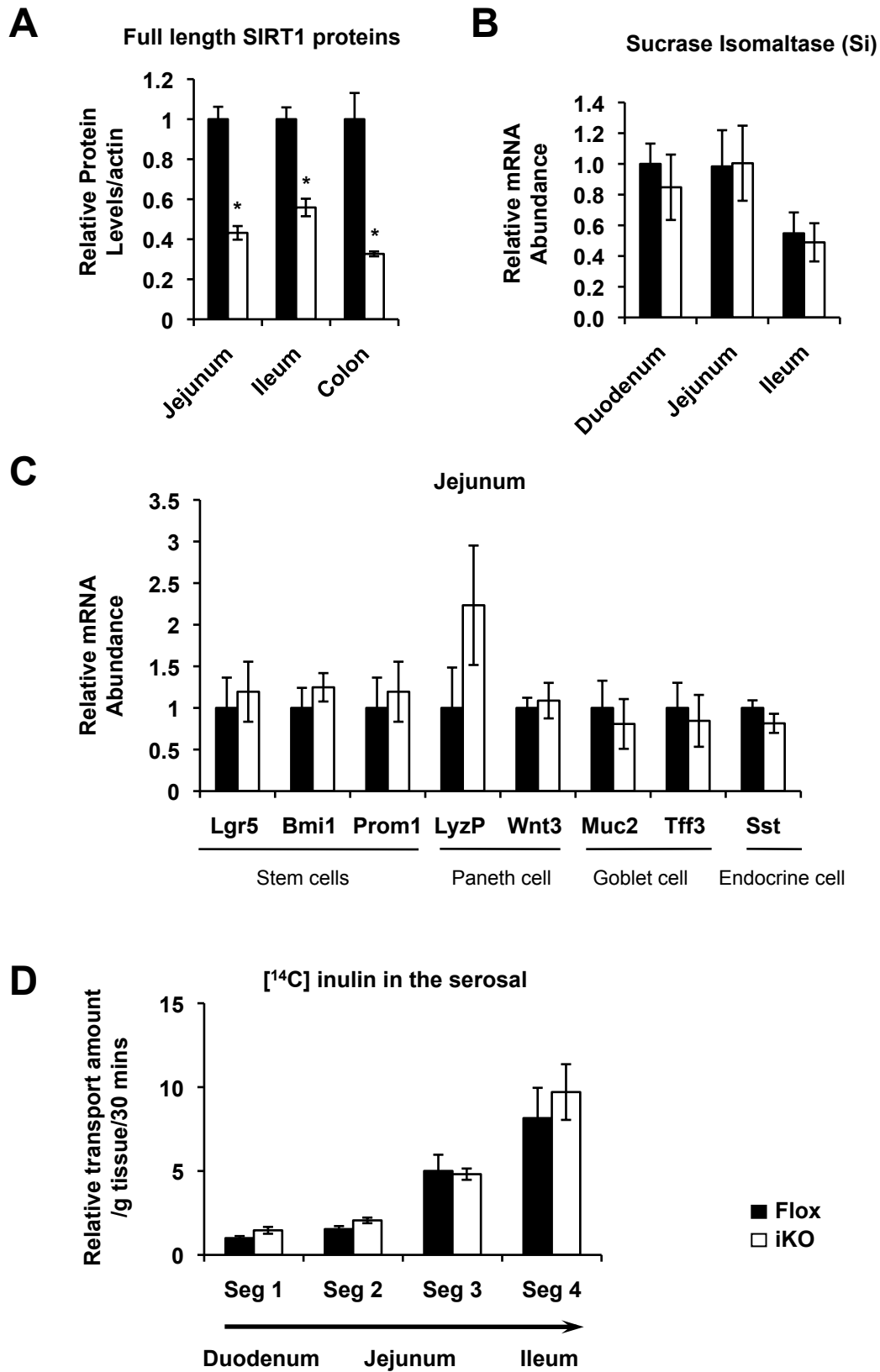
feeding. Top two panels, microvesicular hepatic steatosis lesions primarily involved zones 2 and 3; Bottom two panels, steatohepatitis lesions characterized by numerous multifocal lipogranulomas (arrows) and multinucleated giant cells (macrophages) containing abundant lipids and pycnotic hepatocytic nuclei (arrow head). (D) SIRT1 iKO mice display increased hepatic levels of triglycerides after 7 weeks of LD feeding (n=6-8). (E-F) Feces of SIRT1 iKO mice have a slightly reduced level of cholesterol (E) while a normal bile acid content (F) after 7 weeks feeding of LD. *p<0.05, # 0.05<p<0.10.

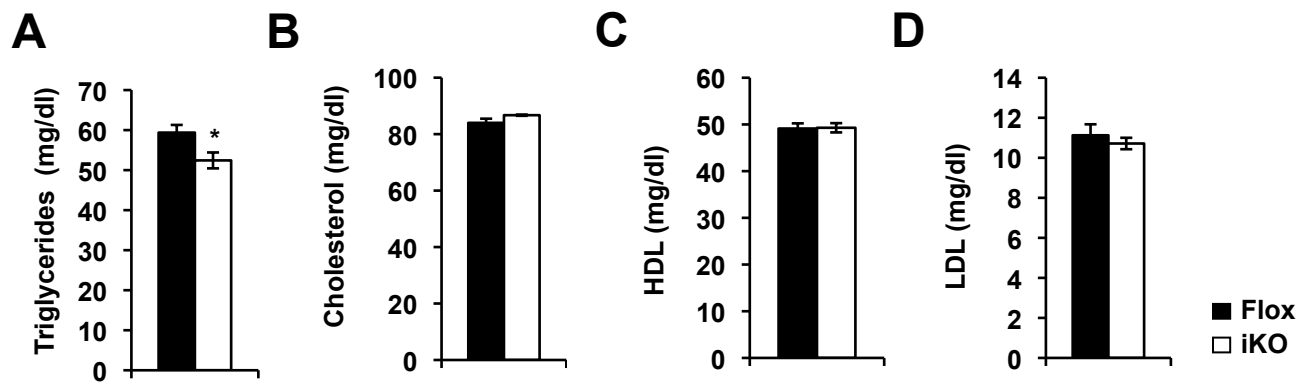
Figure S8 Villin-Cre mice have normal bile acid metabolism. (A) Villin-Cre mice have normal serum bile acid levels on a chow diet (n=4-5, # 0.05<p<0.10). (B) Villin-Cre mice have normal serum bile acid levels after an 11-day feeding of CA diet (n=2-9, # 0.05<p<0.10). (C) Villin-Cre ileum have normal mRNA levels of genes involved in bile acid and cholesterol metabolism on a chow diet (n=5-6). (D) Villin-Cre mice have normal ileal FGF15 levels on a chow diet (n=4-7). (E) Villin-Cre mice have normal hepatic mRNA levels on a chow diet (n=4-7, *p<0.05). All animals are age-matched females except (A). The exact animal number in each group was labeled on the bars in panels (A), (B), (D), and (E).

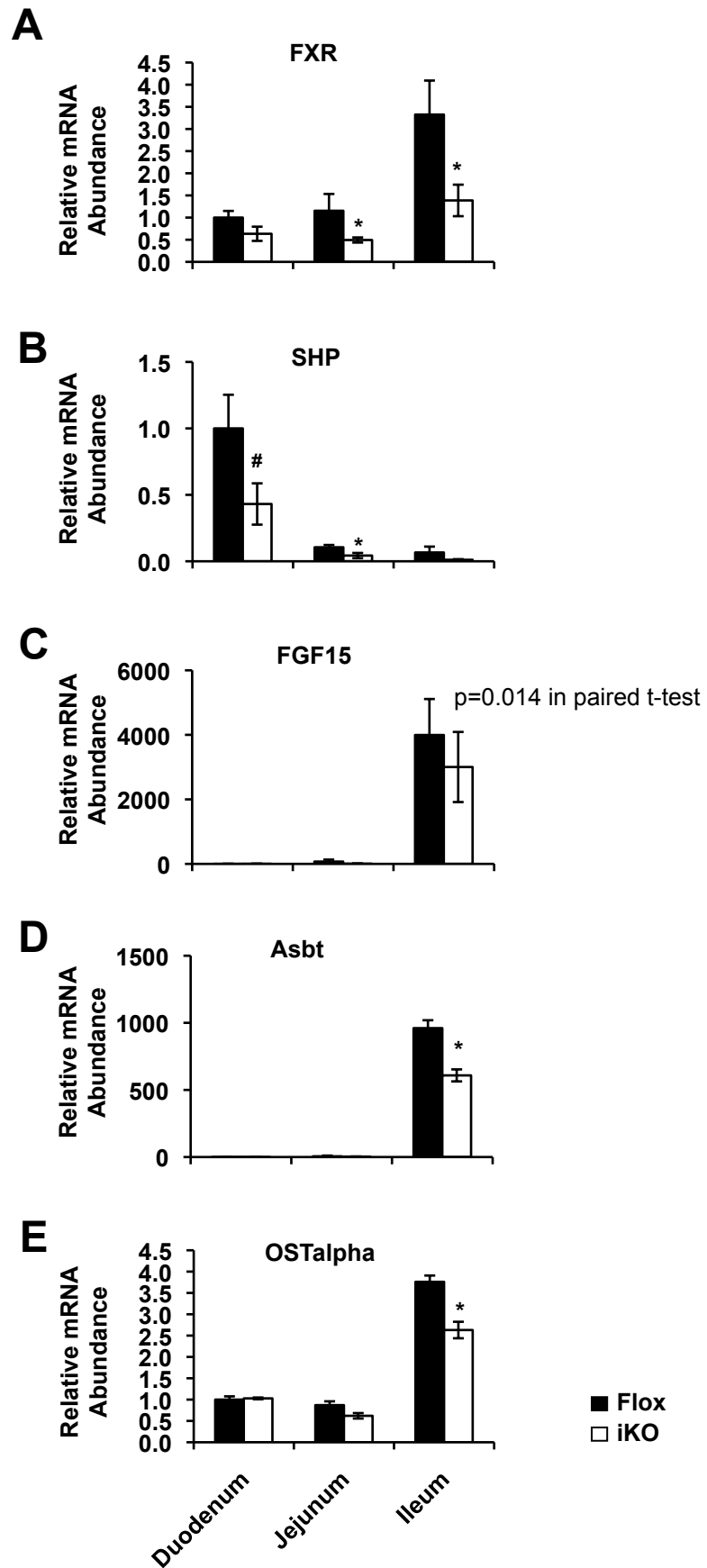
References:

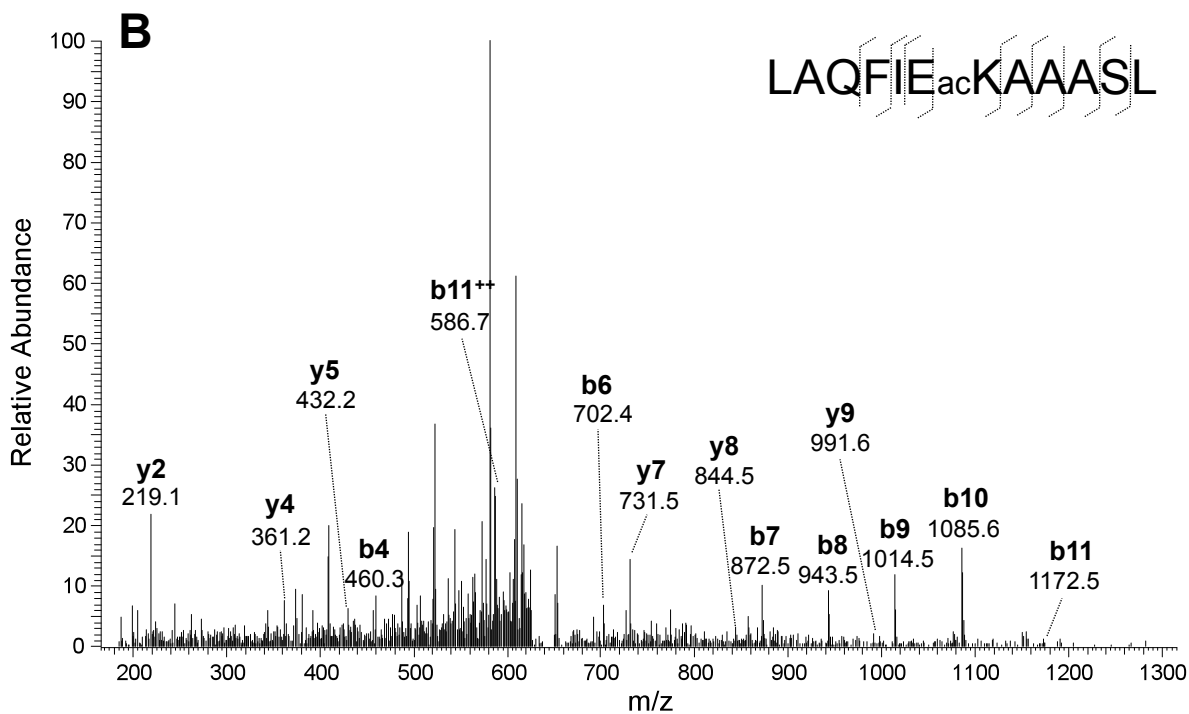
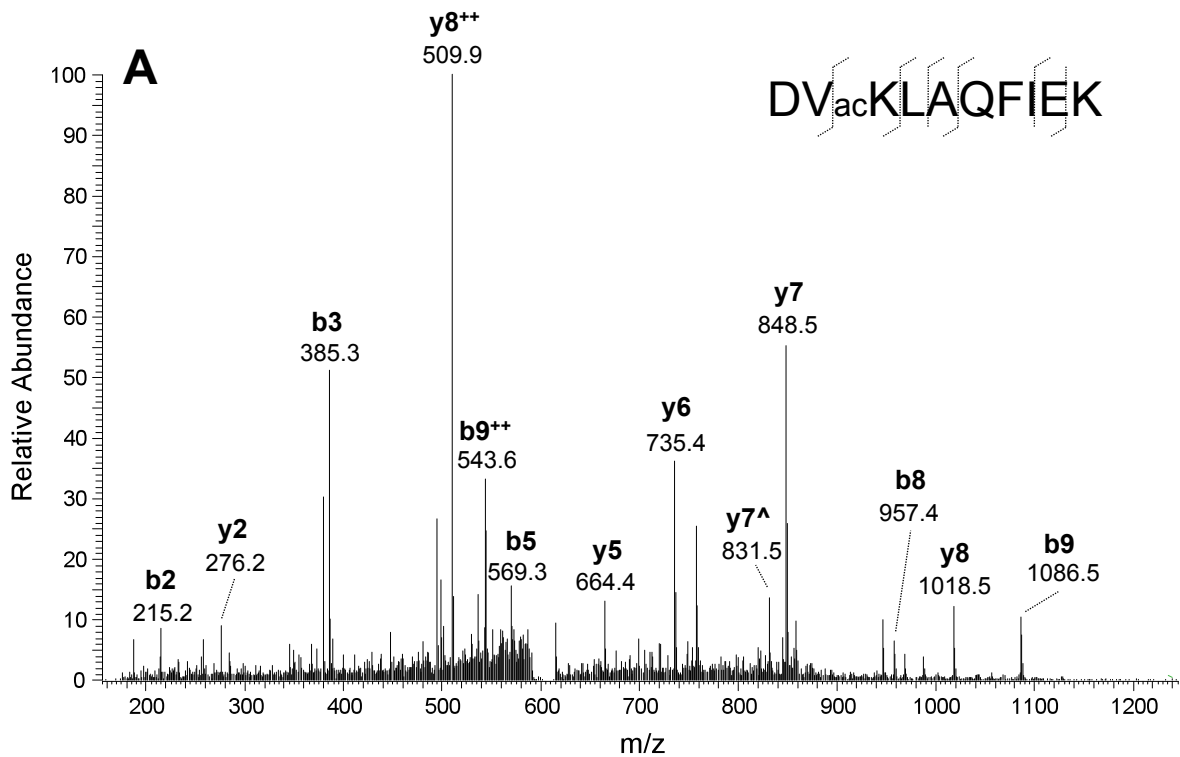
1. Kleiner, D. E., Brunt, E. M., Van Natta, M., Behling, C., Contos, M. J., Cummings, O. W., Ferrell, L. D., Liu, Y. C., Torbenson, M. S., Unalp-Arida, A., Yeh, M., McCullough, A. J., and Sanyal, A. J. (2005) Design and validation of a histological scoring system for nonalcoholic fatty liver disease. *Hepatology* **41**, 1313-1321

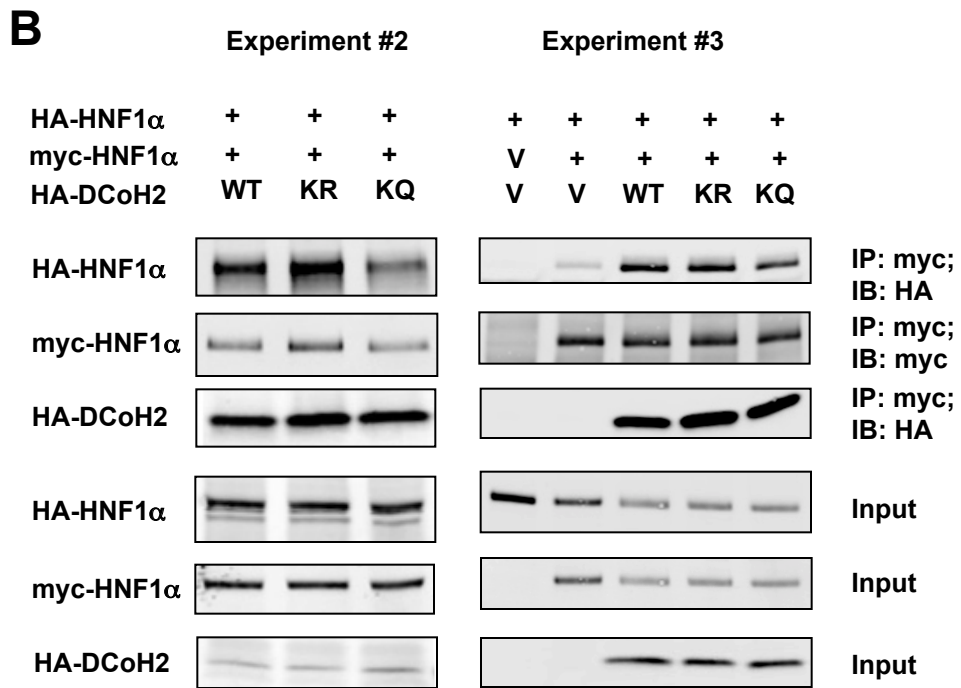
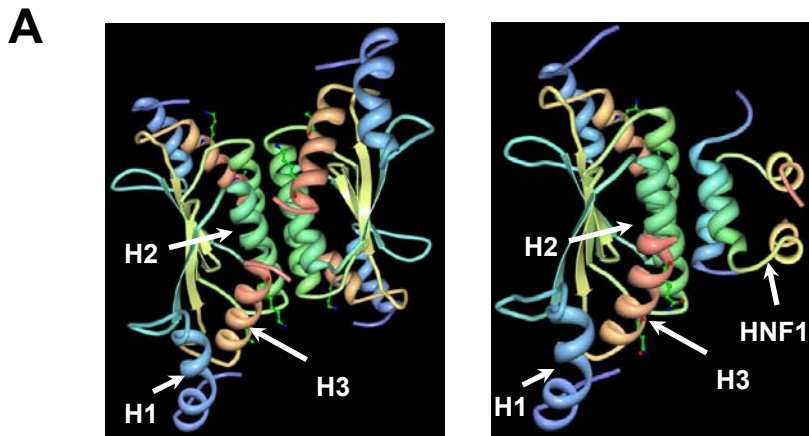
2. Rao, A., Haywood, J., Craddock, A. L., Belinsky, M. G., Kruh, G. D., and Dawson, P. A. (2008) The organic solute transporter alpha-beta, Ostalpha-Ostbeta, is essential for intestinal bile acid transport and homeostasis. *Proc Natl Acad Sci U S A* **105**, 3891-3896
3. Chen, F., Ma, L., Dawson, P. A., Sinal, C. J., Sehayek, E., Gonzalez, F. J., Breslow, J., Ananthanarayanan, M., and Shneider, B. L. (2003) Liver receptor homologue-1 mediates species- and cell line-specific bile acid-dependent negative feedback regulation of the apical sodium-dependent bile acid transporter. *J Biol Chem* **278**, 19909-19916
4. Kim, S. C., Sprung, R., Chen, Y., Xu, Y., Ball, H., Pei, J., Cheng, T., Kho, Y., Xiao, H., Xiao, L., Grishin, N. V., White, M., Yang, X. J., and Zhao, Y. (2006) Substrate and functional diversity of lysine acetylation revealed by a proteomics survey. *Mol Cell* **23**, 607-618
5. Chen, Y., Kwon, S. W., Kim, S. C., and Zhao, Y. (2005) Integrated approach for manual evaluation of peptides identified by searching protein sequence databases with tandem mass spectra. *J Proteome Res* **4**, 998-1005
6. Ma, T. Y., Hollander, D., Erickson, R. A., Truong, H., and Krugliak, P. (1991) Is the small intestinal epithelium truly "tight" to inulin permeation? *Am J Physiol* **260**, G669-676
7. Ma, T. Y., Hollander, D., Erickson, R. A., Truong, H., Nguyen, H., and Krugliak, P. (1995) Mechanism of colonic permeation of inulin: is rat colon more permeable than small intestine? *Gastroenterology* **108**, 12-20
8. Rose, R. B., Pullen, K. E., Bayle, J. H., Crabtree, G. R., and Alber, T. (2004) Biochemical and structural basis for partially redundant enzymatic and transcriptional functions of DCoH and DCoH2. *Biochemistry* **43**, 7345-7355

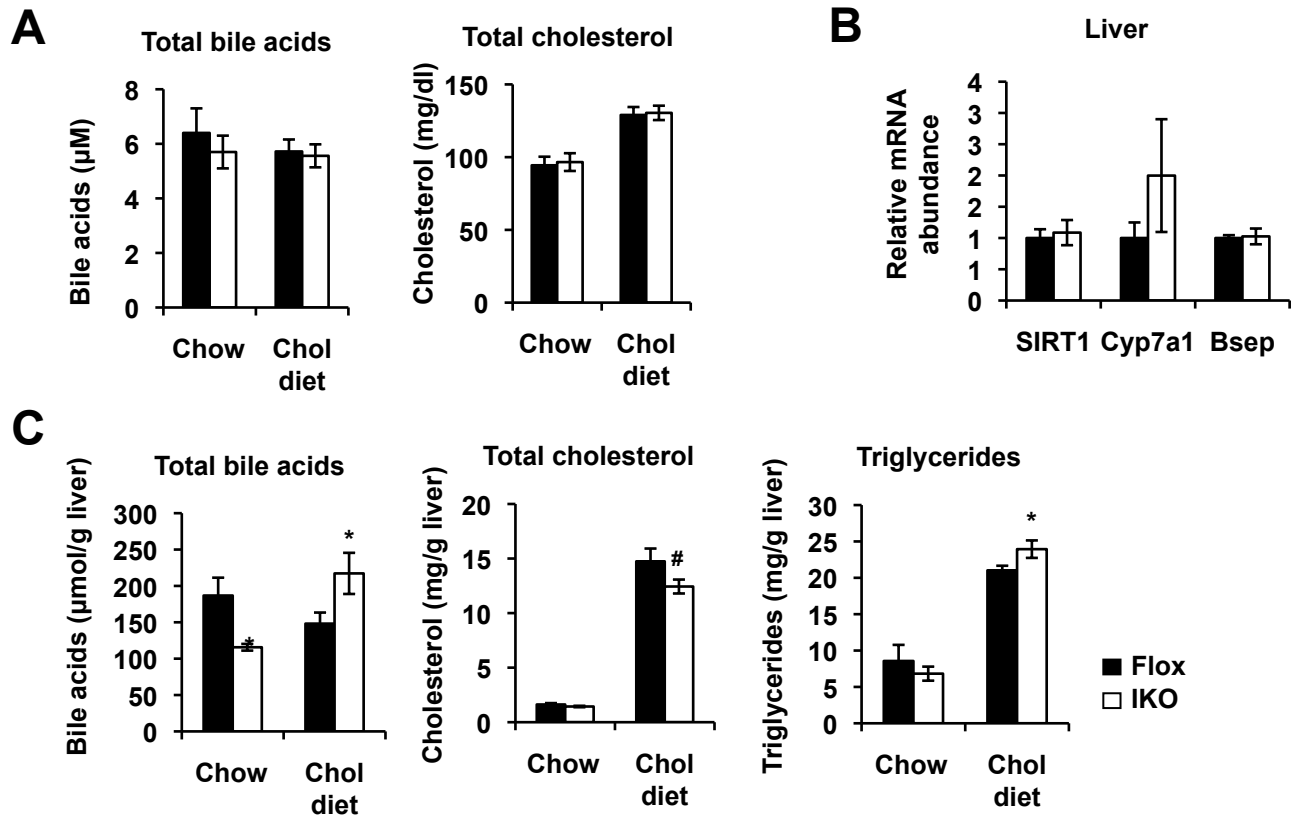


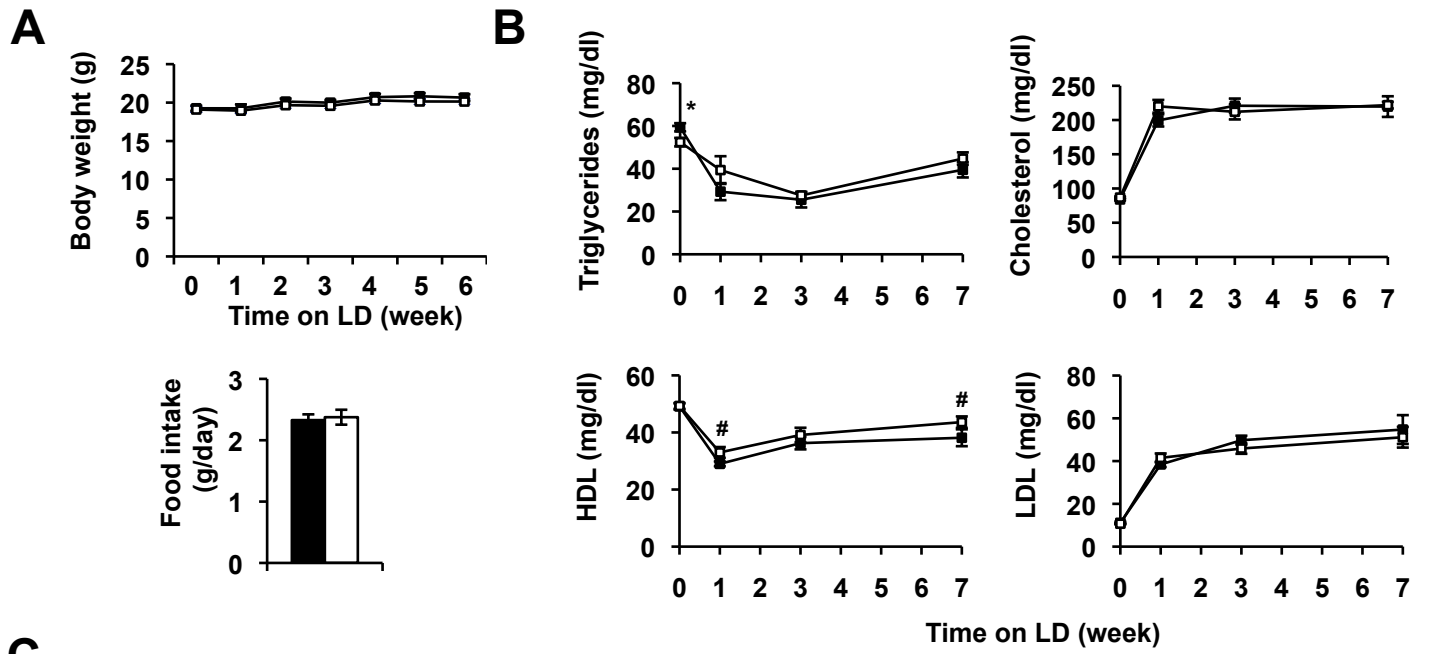




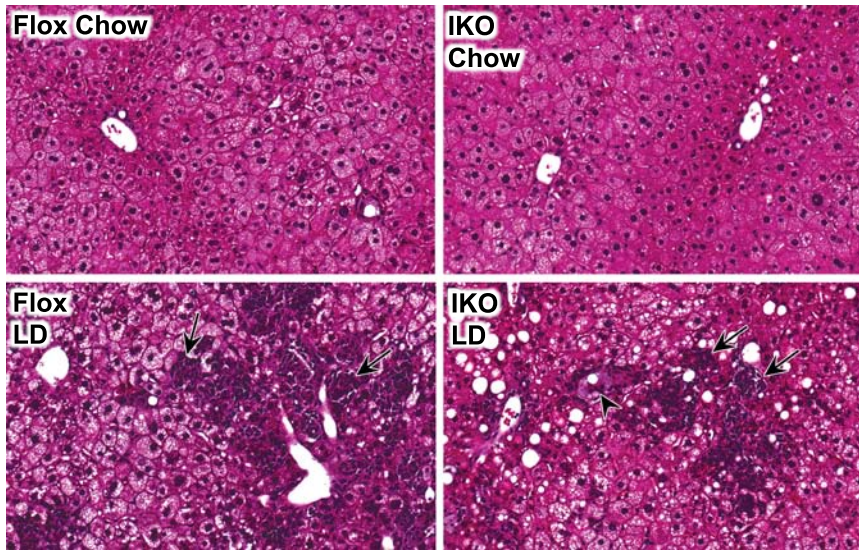




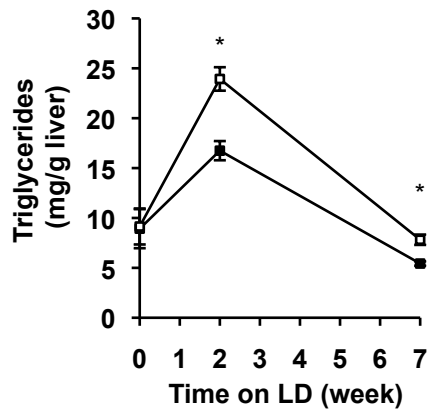




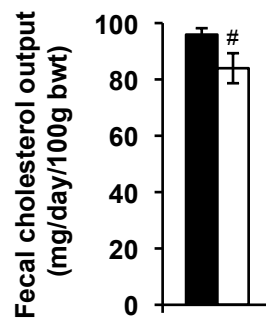
C



D



E



F

